Applied Clay Science 246 (2023) 107189

Contents lists available at ScienceDirect

Applied Clay Science

journal homepage: www.elsevier.com/locate/clay

Research Paper

Bottom up anatase monodisperse nanoparticles grown on sepiolite showing high thermal stability and optimal optical properties for self-cleaning applications

M.F. Acosta [a], M. Morales [b], G. Marcelo [c], S. López-Esteban [b], A. Esteban-Cubillo [d], P.M. Rodríguez-Pascual [b], C. Pecharromán [b,*]

[a] Escuela Politécnica Superior, Universidad Francisco de Vitoria. Crta., Pozuelo-Majadahonda, Km. 1,800, 28223, Pozuelo de Alarcón, Madrid, Spain
[b] Instituto de Ciencia de Materiales de Madrid (ICMM), Consejo Superior de Investigaciones Cientificas (CSIC), C/ Sor Juana Inés de La Cruz, 3, Madrid 28049, Spain
[c] Departamento de Química Analítica, Química Física e Ingeniería Química, Universidad de Alcalá, Alcalá de Henares, 28805 Madrid, Spain
[d] Research and Development Department, Tolsa S. A., Carretera de Madrid a Rivas Jarama, 35, Madrid 28031, Spain

ARTICLE INFO

Keywords:
Sepiolite
Anatase
Nanoparticles
Self-cleaning
Emission spectroscopies

ABSTRACT

Powder samples of anatase monodisperse nanoparticles (np's) have been in-situ synthesized from sepiolite microparticles doped with Ti^{IV}. The role of this clay is double, by one hand, it acts as a chemical reactor, and on the other hand, it becomes a solid substrate for particles, which pin them up avoiding Ostwald ripening process on heating. In this work we show the high thermal stability of these metastable anatase particles up to 850 °C, around 200 °C above the anatase/rutile transformation for ordinary powder particles. Relevant information about the electron bandstructure has been obtained both, by optical diffuse reflectance and emission spectroscopy, which revealed the nature of photon absorption and recombination around the band-gap which determine the utility of this materials as a self-cleaning agent for solid materials.

1. Introduction

Sepiolite is a natural hydrated magnesium clay, with a notable specific surface (around 300 m^2/g) that is being used in multiple industrial applications (Mills et al., 2005; Padmanabhan and John, 2020). These properties are a consequence of its crystalline structure. In fact, although sepiolite (Sep), as well as palygorskite are phyllosilicates, they do not contain continuous planes of SiO_2 tetrahedrons, but, they form blocks of a few polyhedrons along the b axis of the orthorhombic direction (6 SiO_2 tetrahedrons in the case of sep) which extend indefinitely along the c axis. Between these blocks, zeolitic straight channels of 0.4 by 1.1 nm (Brauner and Preisinger, 1956; Preisinger, 1959; Post et al., 2007) run along the c axis. As a consequence, instead of the typical laminar habit of the rest of phyllosilicates, the particles present as elongated tabular aspect as well as a very large specific surface.

On the other hand, Sep has also revealed as a universal host which is able to support many different types of nanoparticles (np's) both metallic (Au, Ag, Cu, Fe, Ni, Pd) or oxidic (ZrO_2, CuO, Fe_2O_3, Fe_3O_4, NiO) (Pecharromán et al., 2006; Tulliani et al., 2007; Esteban-Cubillo et al., 2008a, 2008b; Pecharromán et al., 2009; Esteban-Cubillo et al., 2010; Moya et al., 2011; Pina-Zapardiel et al., 2011; Tiemblo et al., 2012; Pina-Zapardiel et al., 2013). These np's are obtained by a "bottom up" approach on the basis of the ability of interchange Mg^{II} by metallic cations. After controlled heating of these substituted sepiolites, np's spontaneously appear. This procedure has notable advantages. In the first place, it is extremely flexible, in such manner, that it only requires a soluble salt of the desired cation to produce oxidic or metallic np's supported on silicate particles. Additionally, it has been shown that, depending on the synthesis conditions, it is possible locate np's at the Sep surface or inside. In this later case, it was possible to produce stable metallic np's (such as n-Fe, n-Co or n-Ni) that do not present corrosion or oxidation processes even in open environments (Pecharromán et al., 2006; Esteban-Cubillo et al., 2008a, 2008b; Esteban-Cubillo et al., 2010). In this work, we have employed this methodology to obtain anatase np's, the metastable phase of TiO_2 with relevant photocatalytic activity.

Titania np's are currently being used for a large number of industrial applications mainly as whitening agent and photocatalyst and for self-cleaning and/or photocatalysis (Mills et al., 2005; Folli et al., 2009; Hernández-Alonso et al., 2009; Liu et al., 2010; Henderson, 2011; Pelaez

* Corresponding author.
E-mail address: cpg@icmm.csic.es (C. Pecharromán).

https://doi.org/10.1016/j.clay.2023.107189
Received 30 August 2023; Received in revised form 24 October 2023; Accepted 24 October 2023
Available online 1 November 2023

et al., 2012; Katal et al., 2020; Padmanabhan and John, 2020; Alsheheri, 2021). For this later application, only the metastable phases of TiO_2, (anatase and brookite) have a remarkable photocatalytic activity. In fact, according to the literature, metastable phases transform into rutile at temperatures above 600 °C (Gouma and Mills, 2001; Hanaor and Sorrell, 2011; Zhang et al., 2017). However, a detailed thermodynamic analysis determines that metastable phases are stabilized at room temperature (r.t.) by surface energy (Navrotsky, 2003). That means that anatase np's irreversibly transform into rutile, not by a direct thermal process, but for a reason of grain growth. As titania nanopowders are usually obtained in amorphous state at r.t, thermal processes are required to increase the crystallinity and consequently, to improve the photocatalytic response. So that, the anatase/rutile transformation limits the quality of photocatalytic powders. However, isolated np's cannot grow, but they require to be in close contact with other particles. Under these circumstances, Ostwald ripening (Voorhees, 1985) mechanisms take place driven by ion diffusion mechanisms at the particle interface. Therefore, as this process requires that, np's be in close contactthermal treatements on powders aggregates result in the particle enlargement, reducing the specific surface energy, to transform anatase crystals np's into large rutile crystals. Consequently, the addition of dispersant agents, which prevent this transformation, should notably increase the thermal stability range. Nevertheless, most of the available additives contain organic molecules, so that they are unsuitable to be used for thermal treatments. In this sense, the best solution to keep np's isolated is to strongly attach them into a solid substrate. Since bulk materials presents limited values of specific surface, and therefore a scarce number of nucleation centres, a better target to be used will be microparticles. If they are, at least, one order of magnitude larger than np's, the interaction energy allows a simple handling and if the present a large specific surface plenty of available contact spots for np's binding will be available, and the np's content in the micro-nano composite will be larger (Pecharroman et al., 2007).

Additionally, this micro-nano composites also solve one of the key problems of np's handling. Up to date, many efforts have been made to avoid loose np's that could be inhaled, decreasing toxicity, and thus improving safety for health. An example is a low melting point glass that adheres TiO_2 np's (Lopez-Esteban et al., 2021). Another approach is the functionalization of anatase with large inorganic particles, which easily increases, at least one order of magnitude, the aerodynamic diameter, so that this process limits its possible dispersion in air through dust clouds. Therefore, the dispersion of nanopowders into larger microparticles hinders the risk of nanomaterial intake by inhalation (Pecharroman et al., 2007).

Another positive outcome of the micro-nano configuration is the easiness of recyclability. As well as the application of this solution in real environments notably reduces the nanoparticle pollution, the collection process, once it ended its useful life, is quite simple. Just washing the product with water, the product can be simply recover by conventional filtration.

From all the possible powdered matrices, Sep has been one of the chosen for supporting anatase np's due to its large surface area, the microstructure and its rheological properties (Aranda et al., 2008; Nieto-Suárez et al., 2009; Alvarez Berenguer, 2013; Zhou et al., 2017; Katal et al., 2020; Sturini et al., 2020; Vaquero et al., 2020). In all these cases, the approach can be considered to be "top-down", as it is necessary to obtain np's to posteriorly attach them to the matrix. In this sense, due to the lack of Ti^{IV} soluble salts, high melting point and the required small size, synthesis methods for anatase at a large scale are limited to those using a few number of reagents, (Yang et al., 2008; Liu et al., 2010; Pelaez et al., 2012; Horti et al., 2019; Padmanabhan and John, 2020; Alsheheri, 2021). In this context, the introduction of new scalable procedures may have a large industrial impact. Methods that avoid the strong aggregation tendency of np's are especially sought for the purpose of preserving the photocatalytic activity.

In this work, we describe a synthesis method that produces monodisperse anatase np's on the surface of Sep microparticles from a "bottom up" methodology. The inert nature of this clay, its large specific surface, and its thermal stability until temperatures of 850 °C, turn it into a thermally stable dispersant. In this manner, the present method opens a doorway for the improvement and harnessing of the TiO_2 dry powder photocatalytic behaviour. The employed synthesis method is an adaptation of a more general procedure that has been found to be able to produce a large panoply of different materials(Pecharromán et al., 2006; Pina-Zapardiel et al., 2013). In all cases, np's present a remarkable chemical and thermal stability, as well as a very small size (<15 nm) and a very good monodisperse character. A complete microstructural and spectroscopic characterization of the electronic properties of such np's has been carried out on samples heated at temperatures up to 1000 °C in order to precisely determine the transformation anatase/rutile points.

2. Experimental section

Natural sepiolite mineral from Vicalvaro-Vallecas (Tolsa, Spain) has been purified and micronized by a wet process that allows obtaining a final product with >95% content of Sep (Pangel S9 by Tolsa ®). The sepiolite needle-like particles have a length ranging from 0.2 to 2 μm and a thickness of 20–100 nm. Structural channels of 0.5–1.1 nm extend all along the length of the fibres.

A 5 wt% Sep/water suspension was homogenized in a Silverson high shear mixer to then acidified by H_2SO_4 (Sigma Aldrich) to $pH = 0$. When the strong acid treatment changed the rheology of the suspension (from thixotropic to newtonian), an aqueous dissolution 1 M of hydrated titanium oxysulphate (Sigma Aldrich) were added in an equivalent proportion of 25 wt% of TiO_2. Afterwards, the extremely acid suspension was gradually neutralized by NaOH 1 M dissolution (Sigma Aldrich) up to $pH = 6$, where the suspension recovers its thixotropic behaviour. After removing the sodium/magnesium sulphate by several process of filtration of the suspension, a powder of Ti^{IV}-doped sepiolite was obtained.

The obtained powders were calcined in a conventional furnace, in air atmosphere, at a heating rate of 10C/min, up to the specific temperature (250 to 1000 °C) and maintained for 2 h.

ATD/TG measurement were carried out in a SDT Q600 TA Instruments calorimeter, from room temperature to 1100 °C at a heating rate of 7 °C/min in an air (100 ml/min) atmosphere.

The X-Ray Diffraction analysis were carried out in a Bruker D8 Advance diffractometer. The patterns were recorded over the angular range of $5° - 70°$ (2θ) using Cu k_α radiation. HRTEM micrographs were taken in a JEOL JEM 2100 microscope at ICTS (Centro Nacional de Microscopía Electrónica).

Infrared spectra were collected with a Bruker Vertex V70 at vacuum, from 300 to 4000 cm^{-1} on powdered samples dispersed in KBr. For a sake of comparison, spectra were normalized by dividing the experimental absorbance from the integral of the signal from 900 to 1200 cm^{-1}, corresponding to the Si—O spectral stretching region of Sep.

For the self-cleaning characterization, Rhodamine-B solution at 0.2% in isopropanol from Fluka (PC Code 10627609) was employed. 1.2 ml of this liquid reagent were absorbed by 600 mg of Sep/TIO_2 powders. After drying, dyed powders of samples heated at 25, 400 and 600 °C were uniaxial pressed under 25 MPa to conform pellets. The obtained disks have the required mechanical toughness to be manipulated. Afterwards, they were illuminated with a nearly monochromatic LED at 385 nm with a radiation intensity of 23.4 mW/cm^2, in such manner that light heating effect could be neglected. Diffuse reflectance spectra were taken at different times to evaluate the dye photodegradation using a Jasco V-660 spectrophotometer equipped with a diffuse reflectance attachment. The reflectance spectra were transformed to Kubelka-Munk (KM) units through the relationship, $KM = 2R/(1\text{-}R)^2$ to then deconvolute it into a series of lorentzian curves. From all of the curves, only those located from 400 to 600 nm were taken into account to estimate the rhodamine B degradation. The same experimental equipment was employed for bandgap determination on pure pressed powder pellets.

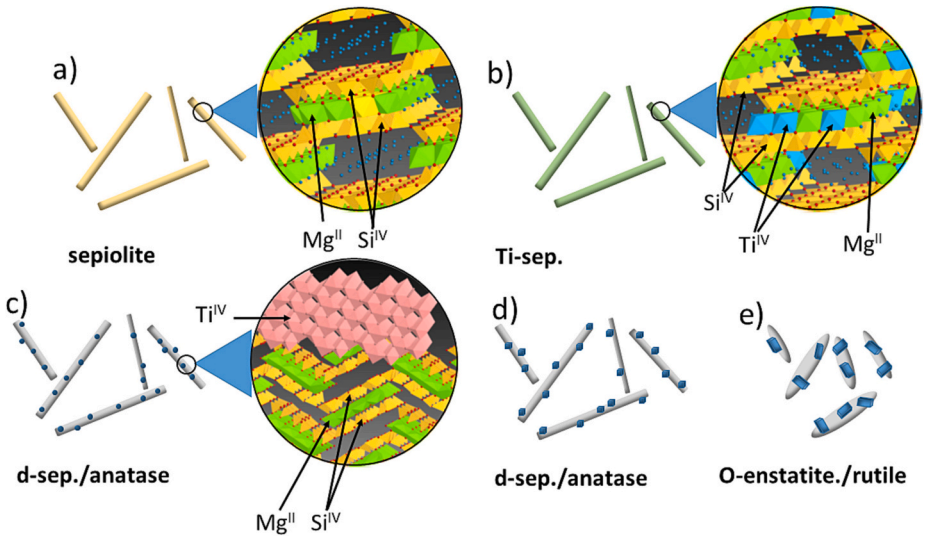

Fig. 1. Schematics of TiO_2/Sep synthesis route. a) Suspension of Sep particles. Insight showing the framework of the crystalline magnesium silicate structure. b) Suspension of Ti^{IV} doped Sep particles. Acid treatment leaches distal Mg^{II} octahedrons which are occupied by Ti^{IV} polyhedrons. Insight showing the framework of the crystalline magnesium-titanium silicate structure; c) Thermal transformation of Sep crystalline structure into dehydrated Sep (d-Sep) and subsequent TiO_2 nucleation; d) anatase crystal growth; e) Sep → enstatite transformation and TiO_2 np's coalescence, grain growth and anatase/rutile transformation.

Steady-state fluorescence measurements were performed by using an SLM 8100 AMINCO spectrofluorometer, equipped with a cooled photomultiplier and a double (single) monochromator in the excitation (emission) path. Slit widths were 4 nm for excitation and emission. Sample pellet were put in cell housing for solids and the angle of incidence was 45°.

3. Results and discussion

3.1. SEP/anatasa synthesis

The employed procedure to obtain TiO_2 np's has been previously described in a previous work (Pecharromán et al., 2006) (Fig. 1). This procedure is radically different from the rest which use the Sep microparticles as a substrate to precipitate titania nanoparticles, previously obtained (Aranda et al., 2008; Alvarez Berenguer, 2013; Zhou et al., 2017; Sturini et al., 2020). By this alternative synthesis method, Sep particles become doped with a metallic cation, (Ti^{IV} in the present work) occupying the crystallographic sites of Mg^{II} by a strong acid treatment followed by a mixing with a dissolution containing the doping cation.

This process starts with an acid activation of the magnesium silicate, at $pH = 0$ with a concentrate strong acid and a controlled precipitation of titanium hydroxide as a precursor in the nucleation centres generated in the silicate structure(Esteban-Cubillo et al., 2008a, 2008b; Alvarez Berenguer, 2013). In the case the new cation is less soluble than Mg^{II} at low pH's, by increasing this values (by controlled addition of a basic dissolution), the new cation will precipitate, preferably at the octahedral

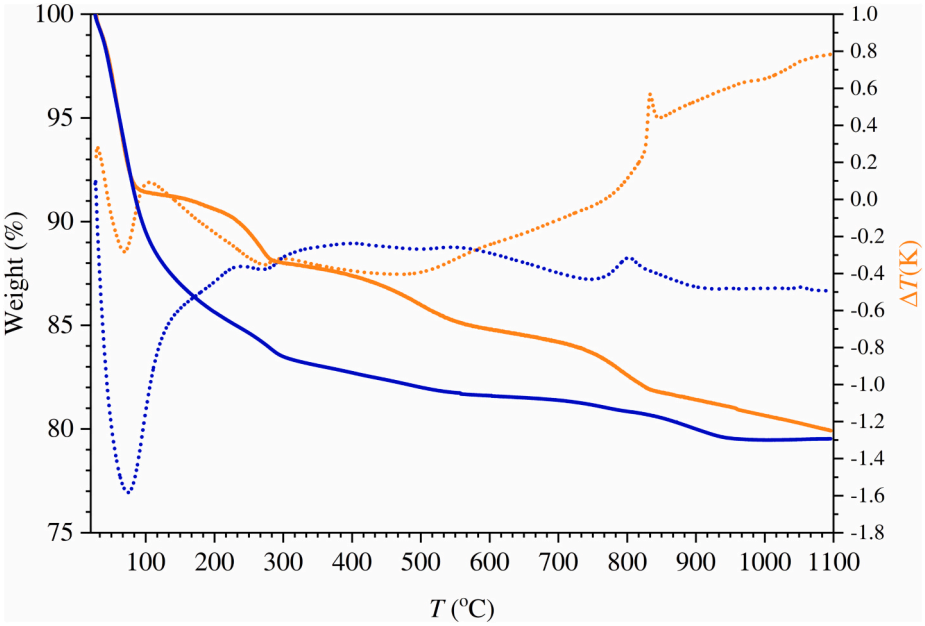

Fig. 2. ATD (dotted lines) /TG (continuous lines) plot corresponding to the Ti^{IV} doped Sep (Blue lines) and natural Sep (orange lines), from r.t. to 1100 °C. (For interpretation of the references to colour in this figure legend, the reader is referred to the web version of this article.)

Mg^{II} crystallographic sites which became vacant by the previous acid treatment. It should be noted, that the obtained powder is Sep from a crystallographic point of view. Only, after the Sep thermal transformation (a phase transition associated to the loss of zeolitic water in the channels that induces a folding of the crystalline structure), nanoparticles of the corresponding cation (or metal in the case of applying a reducing atmosphere) nucleates and grow all along the transformed Sep. Therefore, Sep plays an active role as a chemical reactor as well substrate and dispersant, some of the desired properties to optimize a photocatalytic process.

More specific details using some other cations can be found in the following references (Pecharromán et al., 2006, 2009; Esteban-Cubillo et al., 2008a, 2008b; Esteban-Cubillo et al., 2010; Pina-Zapardiel et al., 2011, 2013). In the present case, doping Sep with Ti^{IV} has become difficult because it requires a soluble salt and Ti^{IV} compounds tend to be highly insoluble. From all the few available options we have chosen titanium oxysulphate, against titanium alkoxides or titanium chloride because of the cost and the ease of handling, which would allow to scale up this process for an industrial production.

3.2. ATD/TG analysis

In Fig. 2 appears the thermal evolution of powder of titanium doped Sep compared with that of pure Pangel S9 Sep (from Tolsa. On heating, sample experiments several weight losses, of 15, 1, 1% and 3.7% at 230320550 and 950 °C respectively (which also appears as minima or maxima into the ATD curve). The first stage may be due to the loss of adsorbed water, while and the second and third processes are customary assigned to the loss of the two type of water molecules contained into the Sep crystalline structure, being the last one associated with the irreversible structure folding. Similar processes take place in the case of pure Sep, but in some cases the temperatures are slightly smaller, and the water loss is not as severe. It may indicate that the loss of Mg^{II} in the strong acid treatment produces a partial decrease of water molecules in the Sep channels, or a partial decomposition of the crystalline structure by substituting a tetravalent cation as it is Ti^{IV} by Mg^{II}. However it should be noted that both materials behaves qualitatively in a similar way, which suggests that the crystalline structure of Sep does not change by the ionic exchange. At larger temperature, a maximum at $T = 802$ °C and a minimum around $T = 920$ °C can be seen into the ATD curve. We assign these features to the enstatite formation, which is a reconstructive crystallographic transformation, which notably distorts the external shape of the microparticles.

3.3. XRD analysis

In our synthesis method, we have lixiviated Mg^{II} cations by reducing the pH of a Sep suspension down to $pH = 0$. Afterwards, a concentrated solution of $TiOSO_4$, was added to, then, rise the pH by means of NaOH. This route is able to dope the crystalline structure of silicate microparticles with Ti^{IV} cations by substituting Mg^{II} at octahedral positions. As a result, a Ti^{IV} doped magnesium silicate, with the crystalline structure of Sep, was obtained, as x-ray diffraction pattern indicates in Fig. 1. Although oxysulphate via is not new (Horti et al., 2019) for anatase synthesis, we use this salt for doping Sep, not for titania synthesis. Doped Sep microparticles are no longer stable at higher temperatures (from 250 to 650 °C). On heating, Sep losses its structural water molecules and the crystalline structure modifies (Perraki and Orfanoudaki, 2008; Hernández-Alonso et al., 2009; Zhang et al., 2017). During this transformation, Ti^{IV} cations are no longer stable as substitutional at the octahedral Mg^{II} sites, and they nucleate as amorphous and isolated titania np's.

In order to determine the thermal stability of such np's, samples were heated at higher temperatures up to 1000 °C. In particular, XRD (Cu k_α radiation) patterns of pressed powder pellets calcined were used to determine the crystalline structure of both, silicate and titania, as a function of heating (Fig. 1). The initial sample ($T = 25$ °C) and the sample heated at 250 °C only show diffraction maxima corresponding to crystalline Sep in addition to some background features, possibly due to the chemical deposition process of TiO_2 in amorphous state. When the calcination temperature rises to 400 °C, the strongest peaks of the anatase appear, while Sep large peak at $2\theta = 7°$ reduces, and a new peak appears at 11°. This is a direct proof of the crystalline transformation by folding of planes parallel to the channels of Sep (Brauner and Preisinger, 1956; Preisinger, 1959; Post et al., 2007), indicating that both, anatase nucleation and Sep transformation processes, are linked.

At 400 °C, nanocrystalline anatase is unambiguously detected. From this temperature to 850 °C, the anatase peaks become sharper, indicating a crystallinity enhancement. However, from 850 to 900 °C all the titania transforms into rutile and this transformation is not due to some reconstructive process of titania, but it is associated to a phase transition in the silicate matrix micro-particles. According to Zhang et al., at $T = 850$ °C (Zhang et al., 2017) magnesium silicate suffers a recrystallization into orto-enstatite. This reconstructive phase transformation in the matrix implies a crystal growth which shifts inclusions or anatase np's to the boundary grain. As the available volume at the peripheral volume of the large silicate crystal is very limited, anatase nanocrystals enter in contact, they coalesce and by an Ostwald-Rippening process, suddenly grow and transform into rutile. It can be seen in Fig. 1 how this process requires some time, because in the case of the sample heated at 900 °C, the XRD shows that the anatase/rutile transformation is still partial, and at 950 and 1000 °C, only the rutile phase can be detected.

It should be pointed out how the phase transformations of TiO_2 in this system are entirely ruled by the crystalline transformation of Sep or magnesium silicate. Therefore, one can conclude that it is not possible to indicate a temperature transformation for the different phases of titania, but it depends on the particle size and of the aggregation state (Gouma and Mills, 2001). By instance, in this system anatase/rutile transformation takes place at 850 °C, while pure anatase powder converts into rutile around 600 °C (Hanaor and Sorrell, 2011).

3.4. IR characterization

Infrared spectroscopy can be very useful for characterizing amorphous as well as the first states of crystallization of solids. In Fig. 4, the spectra of a series of calcined Ti/Sep powders diluted into KBr matrices have been plotted. Additionally, a pure Sep spectrum appears for a sake of reference. In these samples three spectral region can be distinguished, i.e. from 3200 to 3700 cm^{-1}, the spectral region corresponding to the O—H vibrations; from 800 to 1200 cm^{-1}, the region of Si—O stretching; and finally from 600 to 800 cm^{-1} the Fröhlich modes corresponding to anatase (Gonzalez et al., 1997). It should be said that in this spectral region overlaps some of the Si—O bending modes of Sep with the A_{2u} mode (transverse optical, TO, frequency 367 cm^{-1} and longitudinal optical, LO, frequency 755 cm^{-1}) and the high frequency mode of the E_u mode (TO = 435, LO = 876 cm^{-1}) corresponding to anatase.

The spectra do not present relevant changes from that of Sep up to 500 °C. The lack of signal from TiO_2 could be due to the fact that most of the Ti^{IV} occupy the octahedral sites of Sep, or that small nanoparticles are embedded into the Sep particles, so that infrared radiation does not reach such nanoparticles. However, from 500 to 650 °C the three considered spectral regions notably change. In the O—H spectral region, sharp bands, associated to cation-O-H nearly disappear. The four modes corresponding to Si—O stretching modes nearly collapse into a single one, and in the region corresponding to anatase vibration, an extremely wide band appears. At 750 °C the spectral region of anatase reaches a maximum of intensity. As the spectra have been normalized to the integral of the absorbance of the Si—O stretching region, it means that the anatase contribution into the dipolar momentum is larger than that of silicate, probably due to some amorphization in the Sep phase. But for larger temperatures, Si—O stretching region changes again, presenting up to 7 modes. Such fact indicates that crystalline structure of silicate

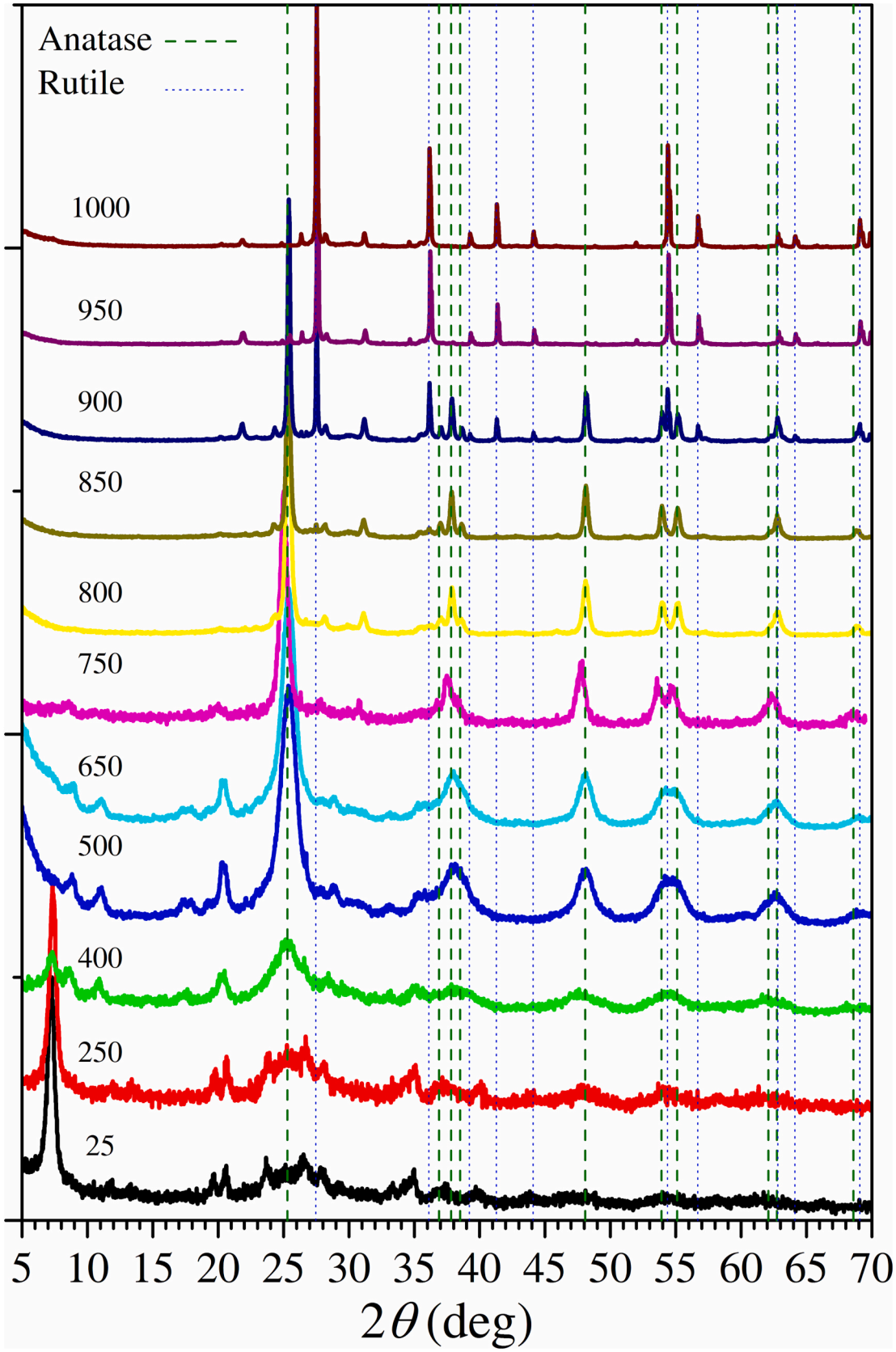

Fig. 3. XRD patterns of the samples showing the evolution of the crystalline phases of TiO_2 as a function of calcination temperature (25, 250, 300, 400, 500, 600, 650, 750, 800, 850, 900, 950 and 1000 °C). As references, we have included vertical lines corresponding to rutile (dotted lines) and anatase (dashed lines).

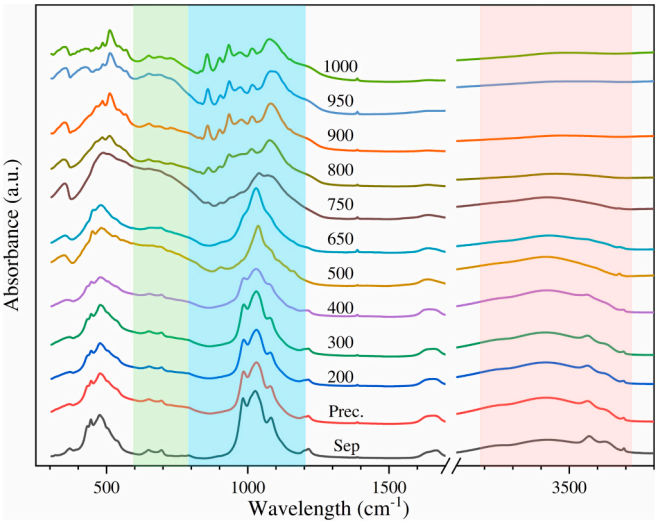

Fig. 4. IR absorbance spectra of the samples showing the evolution of the crystalline phases of TiO_2 as a function of calcination temperature (25, 200, 300, 400, 500, 650, 750, 800, 900, 950 and 1000 ºC). Salmon shadowed region corresponds to OH- and water modes, cyan region is the spectral region of Si—O stretching vibrations and greenish region is the area where Ti—O vibrations may be expected. (For interpretation of the references to colour in this figure legend, the reader is referred to the web version of this article.)

transforms into a totally different crystalline phase (enstatite).

3.5. Electron microscopy characterization

Microstructural characterization of the samples through TEM in a JEOL-200 keV microscope has been performed. The image of the sample without calcination (r.t) appears in Fig. 5a, where deposits of a few tens of nanometres without a defined shape on the magnesium silicate fibres can be observed.

When the sample is calcined up to 250 °C, TiO_2 deposits begin to present contrasts that could be assigned to the formation of small np's of TiO_2 (~ 3 nm) from an amorphous gel, as shown in Fig. 5b. Fig. 5c corresponds to the calcined sample at 500 °C, displaying anatase single crystals. High-resolution transmission electron microscopy (HRTEM, Fig. 6a and b) shows {101} planes indicating the highly crystalline nature. Distance between each crystallographic plane is around 3.5 Armstrong's, as shown in Fig. 6b. Nanoparticle size is around 7 nm and the formation of large clusters is clearly limited, as images reveal in Fig. 3. When the sample is calcined up to 750 °C, anatase single crystals are still visible (Fig. 5d, 6c and d) while silicate fibres appear strongly deformed, because of its thermal transformation and dehydration (Zhang et al., 2017).

3.6. Photocatalytic self-cleaning

In order to explore the possible applications of these powders in self-cleaning applications, a study of the photo-catalytic degradation of

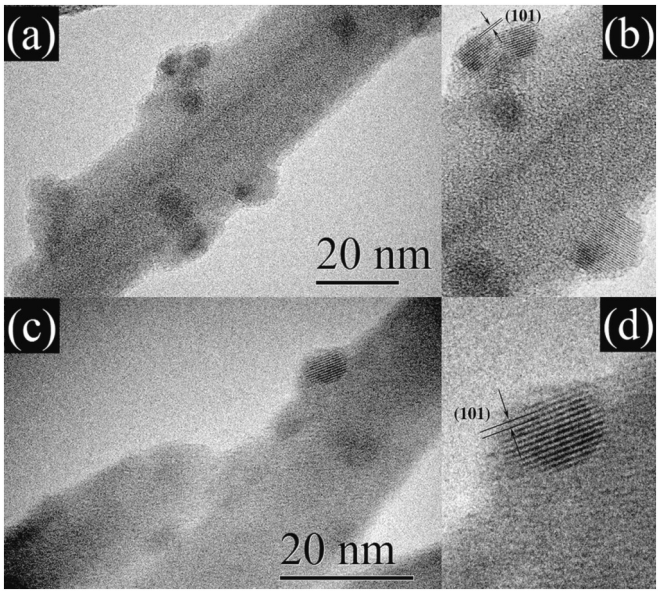

Fig. 6. HRTEM images of magnesium silicate with TiO_2 precipitated via oxysulfphate calcined up to (a)-(b) 500 °C and (c)-(d) 750 °C. Images (b) and (d) are a closer view of (a) and (c), respectively, showing a distance of 3.5 Armstrongs between each crystallographic plane.

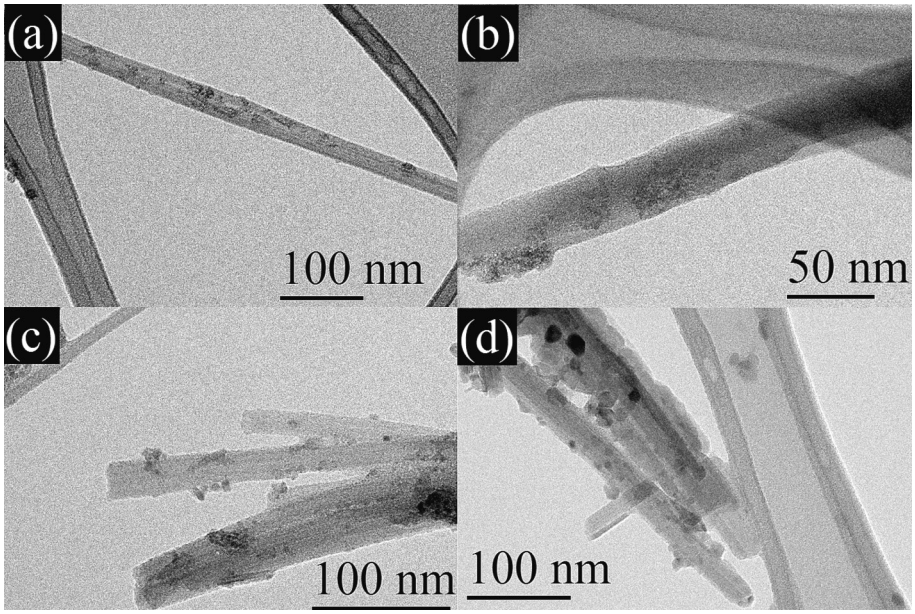

Fig. 5. TEM images of magnesium silicate with TiO_2 precipitated via oxysulfate: (a) without calcination, calcined up to (b) 250 °C, (c) 500 °C and (d) 750 °C.

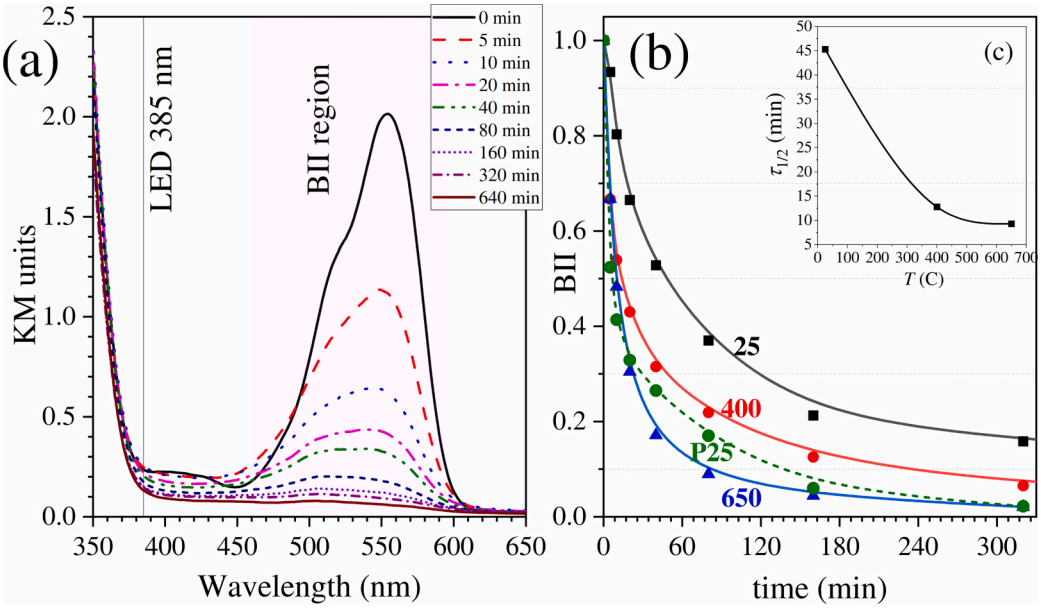

Fig. 7. (a). UV–Vis spectra of Sep/TiO_2 samples (heated at $T = 25$, 400 and 650 °C) with rhodamine-B after different irradiation times with 385 nm LED light. The regions from 400 to 600 nm, labelled as BII, corresponds to absorption rhodamine-B in the visible range. (b) Band Integral Intensity (BII) of diffuse reflectance spectra in KM units of the samples heated at different temperatures: vs. exposition time at 385 nm LED. For a sake of comparison, in green, we have included a commercial sample, Evonik P25 anatase. (c) Inset. Time for 50% degradation of rhodamine-b for for different calcination temperatures.

Rhodamine-B on compact powder pellets was carried out on three selected samples: precursor ($T = 25$ °C), and calcined at 400 °C and 650 °C. Rhodamine B is the reference dye for studying self-cleaning for industrial applications (Ruot et al., 2009) (Italian Standardization Authority (Ente Italiano di Normazione - UNI), 2008). However Rhodamine-B may efficiently absorb light in some spectral ranges in such manner it may spontaneously to degrade (Barbero and Vione, 2016). In order to avoid that, we substituted the commonly employed Ar lamp by a nearly monochromatic 385 nm LED (with a Half width of 10 nm) with relative low intensity (23.4 mW/cm^2). At this wavelength, the Rhodamine-B is nearly transparent but anatase presents a strong (See Supplementary Data).

After irradiation the samples, for increasing time periods from 5 to 320 min, optical spectra of pellets were measured by diffuse reflectance transformed by the Kubelka-Munk procedure into KM units, as it appears in Fig. 7a. Numerical analysis of degradation were made on by fitting the spectra to a sum of lorentizans. Only the two main Rhodamine-B peaks, in the spectral region from 500 to 650 nm were taken into account to determine the degree of degradation (Fig. 7b).

All the samples have measurable photocatalytic activity, even the precursor, which do not seem to include crystalline anatase according to XRD and IR measurements. However, in calcined samples, rhodamine-B degradation occurs notably fast. Quantitatively speaking, in the case of the precursor, we have found a reduction of 50% of rhodamine signal after 45 min of irradiation. This time notably reduces to around 10 min for the samples heated above $T = 400$ °C. The optimal temperature treatment for degradation is 650 °C. However, for higher temperatures, a slight reduction is detected (data not shown), probably due to some change in the matrix microstructure. Finally, above $T > 850$ °C, the conversion of titania into rutile nearly removes all the photocatalytic activity, as expected. For the sake of comparison, we have prepared a powder pellet of pure P25 anatase (Evonik®) dyed and irradiated under the same conditions of the Sep/TiO_2 samples. In Fig. 7b it appears that it presents a similar activity than the sample calcined at 650 °C. In this context, we can conclude that, in dry conditions and for Rhodamine-B self-cleaning application, titania nanoparticles synthesized on Sep behaves, at least, as well as some of the best commercial catalysts.

3.7. Optical band-gap meausurement

Photocatalytic activity is a complex process that requires photons to be absorbed by titania, through electron transitions from valence to conduction bands, to, then, interact with some chemical species. In this regard, the characterization of the energy band-gap of TiO_2 is a crucial question in order to determine both, the crystallographic nature and the photon-electron coupling. Due to the nature of the sample, we have chosen diffuse reflectance UV measurement to, then, transform them via Kubelka-Munk procedure (Džimbeg-Malčić et al., 2011) to relate reflectance spectra to absorption properties. Tauc model states that the absorbance follows a power law:

$$KM{\cdot}E = A\left(E - E_g\right)^{1/\gamma} \quad (1)$$

Where KM, Kubelka-Munk units, are proportional to the optical absorption coefficient, E is the incident photon energy, A is the proportionality constant, E_g is the gap energy and $\gamma = 1/2$ or 2 a coefficient which changes for direct and indirect electron transition, respectively. Reflectance spectra of Sep/TiO_2 pressed powder pellets in Kubelka-Munk units, heated from room temperature up to 1000 °C appear in Fig. 8a.

In order to determine the band-gap energy of direct and indirect transitions, two representations with the following magnitudes at the y-axis, $(KM{\cdot}E)^{1/2}$ and $(KM{\cdot}E)^2$, where plotted vs. E in Fig. 8b (indirect band gap) and Fig. 8b (direct band gap). In both cases, the low frequency region was used to determine the baseline by a polynomial fitting to, then, use these curves to correct the baseline (Makuła et al., 2018). In each case, we can recognize a very definite spectral region where to get a linear fit (Fig. 8a, and b). It should be said that the regions of the two different plots do not overlap. As a result, the crossing of the linear fit with the x-axes determines the values of the direct and indirect transitions. For the temperature range from $T = 200$ to 850 °C, we got a nearly constant energy gap of 3.6 and 3.2 eV for direct and indirect transitions, respectively. At higher temperatures, both energies reduce to 3.2 and 2.95 eV, respectively. Values of energy band gap vs. temperature are plotted in Fig. 6c (black squares for direct band gap and red circles for indirect band gap). These values agree remarkably well with the band gap values of rutile (Daude et al., 1977). The trend while increasing the

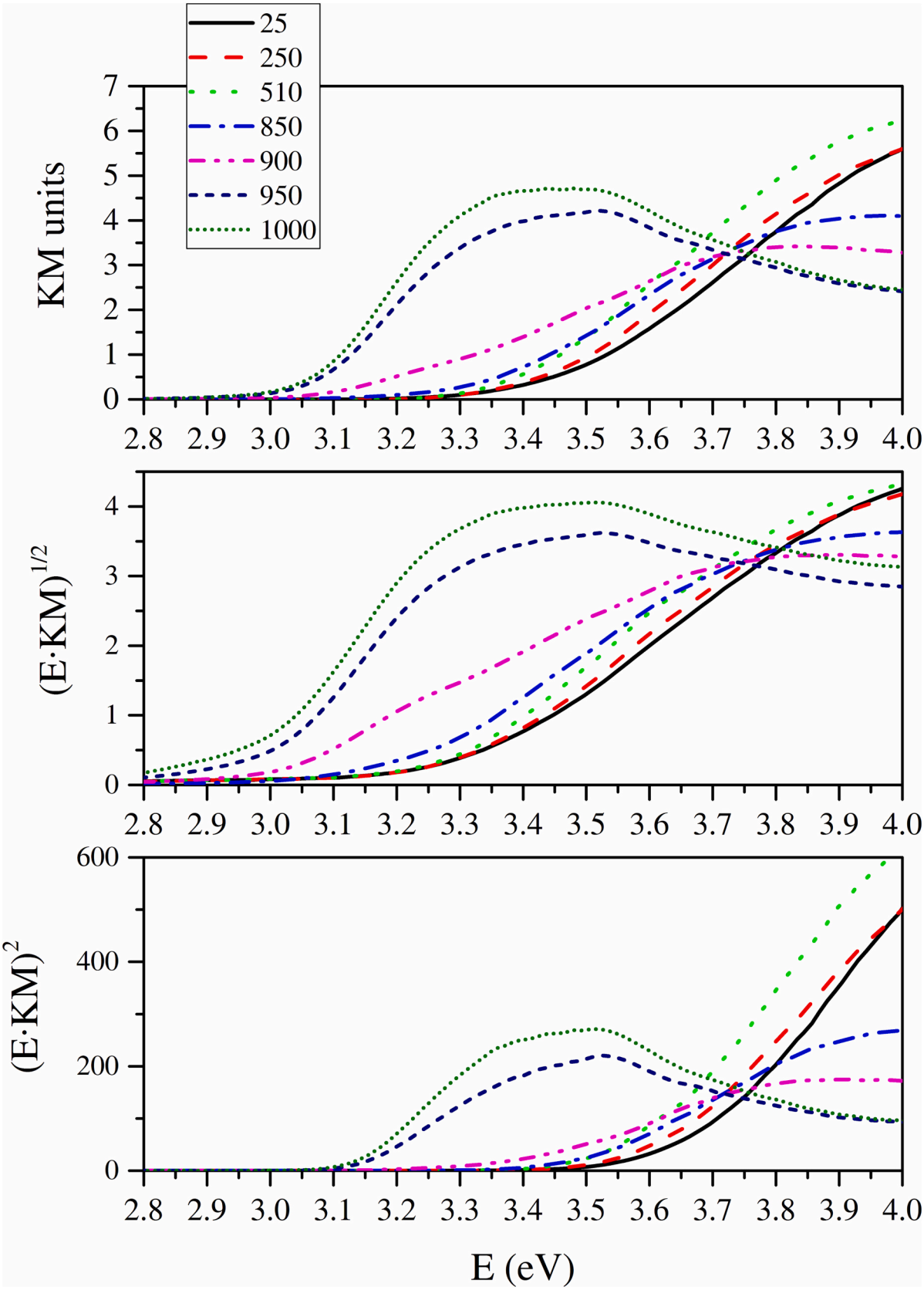

Fig. 8. Optical spectra from diffuse UV–Vis reflectance measurements in different representations to be used for the Tauc model: a) *KM* units; b) $(KM{\cdot}E)^{1/2}$ corresponding to indirect band-gap; c) $(KM{\cdot}E)^2$ for direct band-gaps, plotted vs. *E* (eV) at different heating temperatures (T = 25, 250, 510, 850, 900, 950 and 1000 °C as it appears in the legend). (For interpretation of the references to colour in this figure legend, the reader is referred to the web version of this article.)

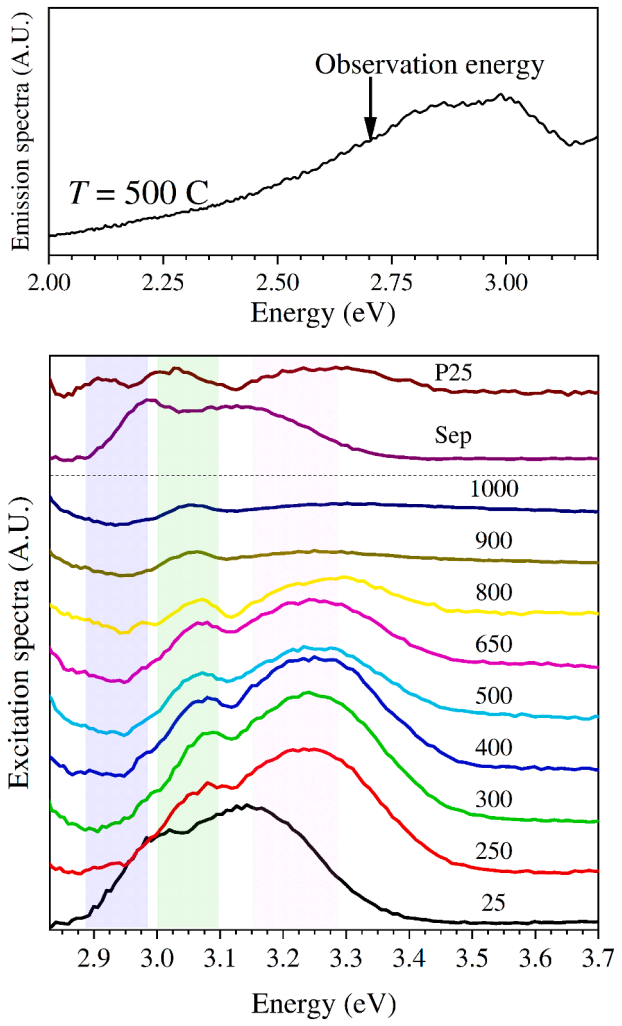

Fig. 9. Graph (a) shows photoluminescence emission spectra of a TiO_2 on calcined magnesium silicate sample at T = 500 °C calcination temperature when excited at a fixed wavelength of 380 nm (3.2 eV). Graph (b) shows photoluminescence excitation spectra at a fixed emission of 480 nm (2.6 eV) for TiO_2 on magnesium silicate sample calcined at different temperatures (T = 25, 250, 300, 400, 500, 650, 800, 900 and 1000 °C).

temperature observed by diffuse reflectance spectroscopy is quite similar to that of XRD for the anatase/rutile transformation. Moreover, while XRD determine an anatase/rutile mixture at T = 900 °C, Tauc-plot analysis shows that the spectrum at this temperature seems to be a mixture to that of 850 and 950 °C.

3.8. Electron bands determination by luminiscence excitation spectroscopy

Photoluminescence spectra can also be useful to gain information about electronic properties. In the case of wide gap semiconductors, as is the case with titania, emission spectra are related with electron allowed decays from conduction to valence bands or to local states into the bandgap due to crystal defects. On the other hand, excitation spectra are mostly related to energy absorption from valence to conduction band. In this later case, due to the nature of the electron transition, selection rules are not so restrictive, so that excitation spectra are strongly related to photon absorption. However, while absorption describes how light is attenuated along the sample, excitation spectra give information about the total amount of photon capture. Although both processes are similar for low absorption (linear approximation), once sample becomes opaque, linear properties overestimate photon capture. In this work, we are going to employ excitation measurement to stablish the spectral photon absorption rate around the bandgap, which is one of the more determining factors in photocatalysis processes, for all the samples.

Luminescence measurements are routinely done on homogeneous materials, as thin films or single crystals. However, powdered samples are challenging samples, because of the strong light scattering that high refractive index contrast (Pallotti et al., 2017) introduces, as is the case of titania np's in air. In some of the previous experiments with dense rough samples, we could see how this scattered were larger than photoemission. Therefore, in this work we have employed a previously described procedure (Pecharroman and Iglesias, 1994), powder compression by optically polished zirconia dies, which notably reduces the surface scattering and allows to obtain nearly specular surfaces on pressed powder pellets,.

The emission spectra of all the samples were taken from 2 to 3 eV with excitation at 3.2 eV. In Fig. 6a, only one curve has been plotted (T = 500 °C), because all the samples look quite similar and they have not any specific feature, apart from a broad and continuous emission band (Fig. 9a). As both anatase and rutile have indirect band-gaps, the light emission from valence to conduction band transition is negligible, so that only transition to or from localized states in the band-gap due to crystalline defects will present some luminescence. In our case, the recorded luminescence is a broad feature which can be assigned to shallow traps due to oxygen vacancies or Ti^{III} (Mercado et al., 2012). As XRD diffractograms (Fig. 3) show, for higher calcination temperatures, crystallinity increases, so that defects concentration diminishes and consequently this emission reduces to nearly disappear around T > 1000 °C (data not shown).

Although emission spectroscopy does not supply much information on these samples, we have found that excitation spectra (Pallotti et al., 2017; Gallart et al., 2018) is a valuable tool to understand the electronic properties of anatase nanoparticles. We have selected the emission at 480 nm (2.7 eV) as a light probe corresponding to transitions from the conduction band to shallow traps into the bandgap. The recorded excitation spectra appear at Fig. 9b. The first obvious conclusion is that excitation data are much less sensitive to light scattering, and they present definite maxima. For a sake of reference, pure Sep and commercial anatase spectra (Evonik® P25) were also included in Fig. 9b. P25, which is a combination of anatase and rutile, presents an excitation spectrum with three maxima at 3.29, 3.01 and 2.91 eV, which has been assigned to indirect band transitions of both rutile and anatase (Daude et al., 1977; Kernazhitsky et al., 2014; Alsheheri, 2021)In the case of Sep, it presents two bands in the considered spectral range at 3.14 and 3.00 eV. Additional measurements (data not shown) allowed us to attribute these maxima to some impurities of iron oxide (~5%), a natural doping of this mineral.

The excitation spectrum of the non-calcined sample (T = 25 °C) looks very similar to that of Sep. This is in good agreement with XRD data (see Fig. 1), as they show that unheated samples present the same crystalline structure as undoped Sep. This is a relevant result because it indicates that Ti^{IV} cations play the same role as defects, as Fe^{III} cations do on raw material, that is, they act as substitutional cations in Sep. However, just by heating at 200 °C, the excitation spectrum changes to be similar to that of anatase, with maxima around 3.24, 3.08, and 2.98 eV. It should be reminded that such diffraction maxima are absent at the diffractogram in Fig. 3 for the sample heated at 250 °C, indicating that a large fraction of the Ti^{IV} cations nucleate into small titania nanocrystals, mainly due to the first dehydration process measured by ATD/TG (Fig. 2). The excitation spectra of samples calcined at higher temperatures remain nearly unchanged up to 800 °C. At 900 and 1000 °C, the main maximum at 3.25 eV notably reduces, which seems to indicate that the anatase/rutile transformation is completed, in agreement with XRD in Fig. 1.

Another interesting result is the notable reduction of the intensity of the excitation spectra of samples heated at 900 and 1000 °C. We propose

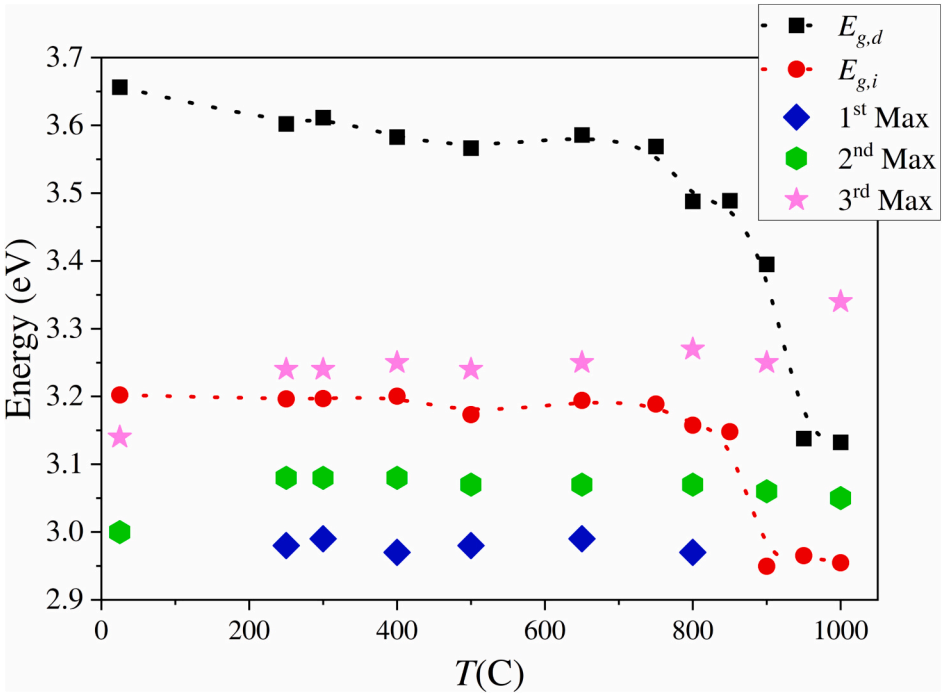

Fig. 10. Band-gap energy vs. Temperature determined from optical measurements (Fig. 8). Black squares stand for direct band-gap transition and red circles for the indirect ones. Additionally, the three maxima values observed in excitation spectra from Fig. 9 (blue diamonds, green circles and pink stars) have been included for each temperature. (For interpretation of the references to colour in this figure legend, the reader is referred to the web version of this article.)

two possible hypotheses. The first one is that luminescence due to shallow traps notably reduces for highly crystallized particles, or that rutile does not absorb light as efficiently as anatase. The first option could be related with the increase of crystallinity of the well-formed rutile crystals. However, a second possibility is also plausible, because the crystallinity of anatase samples is quite high at 800 °C. This latter conclusion could explain why anatase has such a high photocatalytic activity because its electronic configuration favours the radiation absorption at 3.25 eV or 380 nm. If we assume that photoelectrons excited by this radiation are completely thermalized, after the thermalization time, all of them should have energy levels corresponding to a Maxwell-Boltzmann distribution, so that they could take part in photocatalysis reactions or light emission through shallow traps. Consequently, this argument suggests that the optimal wavelength irradiation for this particular sample (Sep-anatase) takes place at 380 nm. Furthermore, excitation measurement could be the optimal tool to determine the excitation wavelength for photocatalytic processes of different anatase powders, as cation doped titania, graphene/anatase composites, etc.

It is also worthwhile to compare these results with that of diffuse optical reflectance (Fig. 10). In the case of electron transition, Tauc model determines the lowest energy required to promote an electron from the valence to conduction band, while excitation spectra, especially for indirect gaps, present maxima at energies larger than those determined by Tauc-plots. This is because excitation measurements determine the probability of generation of photoelectrons, and this process depends on the optical absorbance, but also on the density of states at both valence and conduction band. As a result, excitation maxima, especially due to indirect transition, always appear at energies larger than bandgap.

Another interesting question refers to the absence of maxima in excitation spectra associated to direct transitions detected through Tauc plots. At the spectral range of a low energy transition, the material exhibits a low value of the imaginary part of the refractive index, so that photons may enter deeply into the semiconductor and, as a result, large volumes become illuminated. However, for shorter wavelengths, the light absorption increases notably, which can be expressed through a skin depth reduction, so that photons cannot enter into the semiconductor volume, because they are scattered or reflected. Therefore, this radiation has no significant effect on electron transition. In this regard, excitation studies may be an optimal diagnosis tool for determining the optimal wavelength for photocatalysis.

4. Conclusions

We present a chemical way to synthesize anatase np's (3 to 9 nm) well dispersed and thermally stable up to 900 °C. This method also offers a new possibility to solve the current problems related with the handle of this kind of np's. This high thermal stability is a consequence of being stabilized into Sep microparticles so that, once this material destabilizes and transforms into orto-enstatite, its role as scaffold disappears, and anatase np's coalesce to favour the recrystallization into rutile. These powders present a large self-cleaning efficiency for UV radiation for a dye such as Rhodamine-B (Vaquero et al., 2020).

The herewith synthesis employed method has several advantages against the previous top-down approaches. In the first place, it uses the safer and more available Ti^{IV} precursor (Titanium oxysulphate). It should be noted that this reagent is commonly used in processing of titanium ores, so that, handling is well known. Additionally, as the synthesis procedure has not any volume limitation, it can easily scaled-up for industrial production. It is also worth to note, that once the powders are manufactured, they can be handled with standard microparticle powder procedures (much safer and economic than those applicable to nanoparticles). Additionally, it does not suffer from agglomeration troubles and they have a large thermal stability.

Electronic properties measured from optical and luminescence analysis allow us to determine the lowest direct and indirect bandgaps and, more importantly, the spectral variation of light absorption which determines the efficiency of photocatalysis. Up to our knowledge, this is the first time that excitation spectroscopy has been used to characterized dry titania samples, and it indicates how anatase is a larger photon absorber than rutile, which can be related with its larger photocatalytic efficiency.

Author contribution

M.F. Acosta: Laboratory research, Writing.
M. Morales: Laboratory research.
G. Marcelo: Laboratory research, Writing.
S. López-Esteban: Laboratory research, Writing.
A. Esteban-Cubillo: Laboratory research, Writing.
P. M. Rodríguez-Pascual: Laboratory research.
C. Pecharromán: Head of Research, Laboratory Research, Writing.

Declaration of Competing Interest

The authors declare that they have no known competing financial interests or personal relationships that could have appeared to influence the work reported in this paper.

Data availability

No data was used for the research described in the article.

Acknowledgements

The Authors acknowledge the financial support of PID2020-119130GB-I00 project funded by the Spanish Ministerio de Ciencia e Innovación (MCIN) and Agencia Estatal de Investigación (AEI), MCIN/AEI /10.13039/501100011033. We also thank to the Unit of Characterization of Materials of ICMM (IR and Ellipsometry, x-ray Diffraction and Thermal analysis services) as well as the "Centro Nacional de Microscopía Avanzada-CNME" for the HRTEM pictures.

Appendix A. Supplementary data

Supplementary data to this article can be found online at https://doi.org/10.1016/j.clay.2023.107189.

References

Alsheheri, S.Z., 2021. Nanocomposites containing titanium dioxide for environmental remediation. Des. Monomers Polym. 24, 22–45. https://doi.org/10.1080/15685551.2021.1876322.
Alvarez Berenguer, A., 2013. WO2013020972A2. Process for the Preparation of an Additive Comprising Supported and Dispersed TiO2 Particles. WO2013020972A2.
Aranda, P., Kun, R., Martín-Luengo, M.A., Letaïef, S., Dékány, I., Ruiz-Hitzky, E., 2008. Titania–sepiolite nanocomposites prepared by a surfactant templating colloidal route. Chem. Mater. 20, 84–91. https://doi.org/10.1021/cm702251f.
Barbero, N., Vione, D., 2016. Why dyes should not be used to test the photocatalytic activity of semiconductor oxides. Environ. Sci. Technol. 50, 2130–2131. https://doi.org/10.1021/ACS.EST.6B00213/ASSET/IMAGES/LARGE/ES-2016-002135_0002.JPEG.
Brauner, K., Preisinger, A., 1956. Struktur und entstehung des sepioliths. Tschermaks Mineral. Petrogr. Mitt. 6, 120–140. https://doi.org/10.1007/BF01128033.
Daude, N., Gout, C., Jouanin, C., 1977. Electronic band structure of titanium dioxide. Phys. Rev. B 15, 3229–3235. https://doi.org/10.1103/PhysRevB.15.3229.
Džimbeg-Malčić, V., Barbarić-Mikočević, Ž., Itrić, K., 2011. Kubelka-Munk Theory in describing optical properties of paper (I). Teh. Vjesn. 18, 117–124.
Esteban-Cubillo, A., Marco, J.F., Moya, J.S., Pecharromán, C., 2008a. On the nature and location of nanoparticulate iron phases and their precursors synthetized within a sepiolite matrix. J. Phys. Chem. C 112, 2864–2871. https://doi.org/10.1021/jp077173w.
Esteban-Cubillo, A., Pina-Zapardiel, R., Moya, J.S., Barba, M.F., Pecharromán, C., 2008b. The role of magnesium on the stability of crystalline sepiolite structure. J. Eur. Ceram. Soc. 28, 1763–1768. https://doi.org/10.1016/j.jeurceramsoc.2007.11.022.
Esteban-Cubillo, A., Pina-Zapardiel, R., Moya, J.S., Pecharromán, C., 2010. Stabilization of superparamagnetic nickel nanoparticles in a sepiolite matrix. J. Nanopart. Res. 12, 1221–1229. https://doi.org/10.1007/s11051-009-9811-y.
Folli, A., Jakobsen, U.H., Guerrini, G.L., Macphee, D.E., 2009. Rhodamine B discolouration on TiO2 in the cement environment: a look at fundamental aspects of the self-cleaning effect in concretes. J. Adv. Oxid. Technol. 12 https://doi.org/10.1515/jaots-2009-0116.
Gallart, M., Cottineau, T., Hönerlage, B., Keller, V., Keller, N., Gilliot, P., 2018. Temperature dependent photoluminescence of anatase and rutile TiO $_2$ single crystals: Polaron and self-trapped exciton formation. J. Appl. Phys. 124, 133104 https://doi.org/10.1063/1.5043144.
Gonzalez, R.J., Zallen, R., Berger, H., 1997. Infrared reflectivity and lattice fundamentals in anatase TiO 2 s. Phys. Rev. B 55, 7014–7017. https://doi.org/10.1103/PhysRevB.55.7014.
Gouma, P.I., Mills, M.J., 2001. Anatase-to-Rutile Transformation in Titania Powders. J. Am. Ceram. Soc. 84, 619–622. https://doi.org/10.1111/j.1151-2916.2001.tb00709.x.
Hanaor, D.A.H., Sorrell, C.C., 2011. Review of the anatase to rutile phase transformation. J. Mater. Sci. 46, 855–874. https://doi.org/10.1007/s10853-010-5113-0.
Henderson, M.A., 2011. A surface science perspective on TiO2 photocatalysis. Surf. Sci. Rep. 66, 185–297. https://doi.org/10.1016/j.surfrep.2011.01.001.
Hernández-Alonso, M.D., Fresno, F., Suárez, S., Coronado, J.M., 2009. Development of alternative photocatalysts to TiO2: challenges and opportunities. Energy Environ. Sci. 2, 1231. https://doi.org/10.1039/b907933e.
Horti, N.C., Kamatagi, M.D., Patil, N.R., Nataraj, S.K., Sannaikar, M.S., Inamdar, S.R., 2019. Synthesis and photoluminescence properties of titanium oxide (TiO2) nanoparticles: effect of calcination temperature. Optik (Stuttg). 194, 163070 https://doi.org/10.1016/j.ijleo.2019.163070.
Italian Standardization Authority (Ente Italiano di Normazione - UNI), 2008. Determination of the Photocatalytic activity of Hydraulic Binders – Rhodamine Method (in Italian), 11259. UNI.
Katal, R., Masudy-Panah, S., Tanhaei, M., Farahani, M.H.D.A., Jiangyong, H., 2020. A review on the synthesis of the various types of anatase TiO2 facets and their applications for photocatalysis. Chem. Eng. J. 384, 123384 https://doi.org/10.1016/j.cej.2019.123384.
Kernazhitsky, L., Shymanovska, V., Gavrilko, T., Naumov, V., Fedorenko, L., Kshnyakin, V., Baran, J., 2014. Room temperature photoluminescence of anatase and rutile TiO2 powders. JOL 146, 199–204. https://doi.org/10.1016/j.jlumin.2013.09.068.
Liu, G., Sun, C., Yang, H.G., Smith, S.C., Wang, L., Lu, G.Q., Cheng, H.-M., 2010. Nanosized anatase TiO2 single crystals for enhanced photocatalytic activity. Chem. Commun. 46, 755–757. https://doi.org/10.1039/B919895D.
Lopez-Esteban, S., Cabal, B., Borrell, A., Bartolomé, J.F., Fernandez, A., Faraldos, M., Bahamonde, A., Moya, J.S., Pecharroman, C., 2021. Lead-free low-melting-point glass as bonding agent for TiO2 nanoparticles. Ceram. Int. 47, 6114–6120. https://doi.org/10.1016/j.ceramint.2020.10.190.
Makuła, P., Pacia, M., Macyk, W., 2018. How to correctly determine the band gap energy of modified semiconductor photocatalysts based on UV–Vis spectra. J. Phys. Chem. Lett. 9, 6814–6817. https://doi.org/10.1021/acs.jpclett.8b02892.
Mercado, C.C., Knorr, F.J., McHale, J.L., Usmani, S.M., Ichimura, A.S., Saraf, L.V., 2012. Location of hole and electron traps on nanocrystalline anatase TiO $_2$. J. Phys. Chem. C 116, 10796–10804. https://doi.org/10.1021/jp301680d.
Mills, A., Hodgen, S., Lee, S.K., 2005. Self-cleaning titania films: an overview of direct, lateral and remote photo-oxidation processes. Res. Chem. Intermed. 31, 295–308. https://doi.org/10.1163/1568567053956644.
Moya, J.S., Pecharromán, C., Montero, I., Pina-Zapardiel, R., Esteban-Cubillo, A., Reinosa, J.J., Fernandez, J.F., 2011. Fabrication of nanostructured metallized glazes by conventional fast-firing route. J. Am. Ceram. Soc. 94, 2067–2073. https://doi.org/10.1111/j.1551-2916.2011.04399.x.
Navrotsky, A., 2003. Energetics of nanoparticle oxides: interplay between surface energy and polymorphism†. Geochem. Trans. 4, 34. https://doi.org/10.1186/1467-4866-4-34.
Nieto-Suárez, M., Palmisano, G., Ferrer, M.L., Gutiérrez, M.C., Yurdakal, S., Augugliaro, V., Pagliaro, M., del Monte, F., 2009. Self-assembled titania–silica–sepiolite based nanocomposites for water decontamination. J. Mater. Chem. 19, 2070. https://doi.org/10.1039/b813864h.
Padmanabhan, N.T., John, H., 2020. Titanium dioxide based self-cleaning smart surfaces: a short review. J. Environ. Chem. Eng. 8, 104211 https://doi.org/10.1016/j.jece.2020.104211.
Pallotti, D.K., Passoni, L., Maddalena, P., Di Fonzo, F., Lettieri, S., 2017. Photoluminescence mechanisms in anatase and rutile TiO $_2$. J. Phys. Chem. C 121, 9011–9021. https://doi.org/10.1021/acs.jpcc.7b00321.
Pecharroman, C., Iglesias, J.E., 1994. A method for the determination of infrared optical constants from reflectance measurements on powdered samples. J. Phys. Condens. Matter. 6, 7125–7141. https://doi.org/10.1088/0953-8984/6/35/021.
Pecharromán, C., Esteban-Cubillo, A., Montero, I., Moya, J.S., Aguilar, E., Santarén, J., Alvarez, A., 2006. Monodisperse and corrosion-resistant metallic nanoparticles embedded into sepiolite particles for optical and magnetic applications. J. Am. Ceram. Soc. 89, 3043–3049. https://doi.org/10.1111/j.1551-2916.2006.01190.x.
Pecharroman, C., Cubillo, A.E., Torrecillas, R., Moya, J.S., 2007. Micro/nano composites: a simple and safe way to fabricate nanomaterials. Int. J. Nanotechnol. 4, 282. https://doi.org/10.1504/IJNT.2007.013474.
Pecharromán, C., Esteban-Cubillo, A., Fernández, H., Esteban-Tejeda, L., Pina-Zapardiel, R., Moya, J.S., Solis, J., Afonso, C.N., 2009. Synthesis, conforming, linear, and non-linear optical properties of gold nanoparticles-sepiolite compacts. Plasmonics 4, 261–266. https://doi.org/10.1007/s11468-009-9101-7.
Pelaez, M., Nolan, N.T., Pillai, S.C., Seery, M.K., Falaras, P., Kontos, A.G., Dunlop, P.S.M., Hamilton, J.W.J., Byrne, J.A., O'Shea, K., Entezari, M.H., Dionysiou, D.D., 2012. A review on the visible light active titanium dioxide photocatalysts for environmental applications. Appl. Catal. B Environ. 125, 331–349. https://doi.org/10.1016/j.apcatb.2012.05.036.
Perraki, T., Orfanoudaki, A., 2008. Study of raw and thermally treated sepiolite from the Mantoudi area, Euboea, Greece. J. Therm. Anal. Calorim. 91, 589–593. https://doi.org/10.1007/s10973-007-8329-8.
Pina-Zapardiel, R., Montero, I., Esteban-Cubillo, A., Moya, J.S., Kaplan, W.D., Paramasivam, T., Pecharromán, C., 2011. Palladium nanoparticles on silica-rich

substrates by spontaneous reduction at room temperature. J. Nanopart. Res. 13, 5239–5249. https://doi.org/10.1007/s11051-011-0508-7.

Pina-Zapardiel, R., Esteban-Cubillo, A., Bartolomé, J.F., Pecharromán, C., Moya, J.S., 2013. High wear resistance white ceramic glaze containing needle like zircon single crystals by the addition of sepiolite n-ZrO2. J. Eur. Ceram. Soc. 33, 3379–3385. https://doi.org/10.1016/j.jeurceramsoc.2013.05.033.

Post, J.E., Bish, D.L., Heaney, P.J., 2007. Synchrotron powder X-ray diffraction study of the structure and dehydration behavior of sepiolite. Am. Mineral. 92, 91–97. https://doi.org/10.2138/am.2007.2134.

Preisinger, A., 1959. X-ray study of the structure of sepiolite. Clay Clay Miner. 6, 61–67. https://doi.org/10.1346/CCMN.1957.0060106.

Ruot, B., Plassais, A., Olive, F., Guillot, L., Bonafous, L., 2009. TiO2-containing cement pastes and mortars: Measurements of the photocatalytic efficiency using a rhodamine B-based colourimetric test. Sol. Energy 83. https://doi.org/10.1016/j.solener.2009.05.017.

Sturini, M., Maraschi, F., Cantalupi, A., Pretali, L., Nicolis, S., Dondi, D., Profumo, A., Caratto, V., Sanguineti, E., Ferretti, M., Albini, A., 2020. TiO2 and N-TiO2 sepiolite and zeolite composites for photocatalytic removal of ofloxacin from polluted water. Materials (Basel). 13, 537. https://doi.org/10.3390/ma13030537.

Tiemblo, P., Benito, E., García, N., Esteban-Cubillo, A., Pina-Zapardiel, R., Pecharromán, C., 2012. Multiscale gold and silver plasmonic plastics by melt compounding. RSC Adv. 2, 915–919. https://doi.org/10.1039/C1RA00873K.

Tulliani, J.M., Naglieri, V., Esteban-Cubillo, A., Pecharromán, C., Moya, J.S., 2007. Iron oxide nanoparticles supported onto sepiolite as novel humidity sensors. In: Materials Science and Technology Conference and Exhibition, MS and T'07 - "Exploring Structure, Processing, and Applications Across Multiple Materials Systems.".

Vaquero, C., Esteban-Cubillo, A., Santaren, J., López de Ipiña, J., Galarza, N., Aragón, G., Múgica, I., Larraza, I., Pina-Zapardiel, R., Gutierrez-Cañas, C., 2020. Exposure assessment during the industrial formulation and application of photocatalytic mortars based on safer n-TiO2 additives. Int. J. Environ. Res. 14, 257–268. https://doi.org/10.1007/s41742-020-00252-7.

Voorhees, P.W., 1985. The theory of Ostwald ripening. J. Stat. Phys. 38, 231–252. https://doi.org/10.1007/BF01017860.

Yang, H.G., Sun, C.H., Qiao, S.Z., Zou, J., Liu, G., Smith, S.C., Cheng, H.M., Lu, G.Q., 2008. Anatase TiO2 single crystals with a large percentage of reactive facets. Nature 453, 638–641. https://doi.org/10.1038/nature06964.

Zhang, Y., Wang, L., Wang, F., Liang, J., Ran, S., Sun, J., 2017. Phase transformation and morphology evolution of sepiolite fibers during thermal treatment. Appl. Clay Sci. 143, 205–211. https://doi.org/10.1016/j.clay.2017.03.042.

Zhou, F., Yan, C., Wang, H., Zhou, S., Komarneni, S., 2017. Sepiolite-TiO 2 nanocomposites for photocatalysis: Synthesis by microwave hydrothermal treatment versus calcination. Appl. Clay Sci. 146, 246–253. https://doi.org/10.1016/j.clay.2017.06.010.